Contrasting geochemical signatures of fluid-absent versus fluid-fluxed melting of muscovite in metasedimentary sources: The Himalayan leucogranites

Li-E. Gao[1]*, Lingsen Zeng[1], and Paul D. Asimow[2]
[1]Institute of Geology, Chinese Academy of Geological Sciences, Beijing 100037, China
[2]Division of Geological and Planetary Sciences, California Institute of Technology, Pasadena, California 91125, USA

ABSTRACT

Most of the Himalayan Cenozoic leucogranites are products of partial melting of metapelite sources. In the Malashan-Gyirong area (southern Tibet), the geochemical compositions of leucogranites define two groups with distinct whole-rock major elements, large ion lithophile elements, rare earth elements, high field strength elements, and Sr and Hf isotope ratios. Based on published experimental results that define generalized melting reactions of metapelitic sources, we infer that these leucogranites are the products of two different types of crustal anatexis: fluid-fluxed melting and fluid-absent melting of muscovite in metasedimentary sources. As compared to the leucogranites derived from fluid-absent melting, those from fluid-fluxed melting have relatively higher Ca, Sr, Ba, Zr, Hf, Th, and light rare earth element concentrations, and Zr/Hf, Eu/Eu*, and Nd/Nd*, but lower Rb, Nb, Ta, and U concentrations, Rb/Sr and $^{87}Sr/^{86}Sr$ ratios, and $\varepsilon_{Hf}(t)$. The geochemical differences can be explained by melting behaviors of major (muscovite, feldspar) and accessory minerals (zircon and monazite) during different modes of crustal anatexis. The systematic elemental and isotopic signatures of different types of crustal anatexis and, in particular, the coupling of major and trace elements that results from common influences on rock-forming and accessory mineral behaviors provide tools with which to refine our understanding of the nature of crustal anatexis.

INTRODUCTION

The Himalayan leucogranites are the products of crustal anatexis and offer an outstanding case study that can be used to formulate and test models for the petrogenesis of granites. Experimental results (Patiño Douce and Harris, 1998; Knesel and Davidson, 2002) and theoretical calculations (Inger and Harris, 1993) suggest that most Himalayan leucogranites are the products of fluid-absent melting of muscovite in metapelitic sources. Many geochemical observations from Miocene Himalayan leucogranites support this view (Harris and Massey, 1994; Zhang et al., 2004; King et al., 2011). Recent and updated studies have demonstrated that Eocene Himalayan granitoids, by contrast, were derived from melting of a source consisting dominantly of amphibolite with subordinate pelitic gneiss (Zeng et al., 2011). In specific regions, fluid-fluxed melting of pelitic sources (Prince et al., 2001) has been reported, including both fluid-fluxed melting of biotite (King et al., 2011) and fluid-fluxed melting of muscovite (Gao and Zeng, 2014). This range of formation mechanisms for various Himalayan leucogranites is required by the large differences among these rocks in major elements, trace elements, and isotopic compositions, as well as mineral assemblages.

Published studies (Knesel and Davidson, 2002; Weinberg and Hasalova, 2015) have pointed out that there are systematic differences in major

*E-mail: liegao09@163.com

elements (K, Na, Ca), large ion lithophile elements (LILEs; Rb, Sr, Ba), and Sr isotopic signatures during distinct episodes of fluid-absent melting and fluid-fluxed melting of a single metapelitic source. However, whether there are also systematic variations in high field strength element (HFSE) and rare earth element (REE) concentrations associated with different melting reactions is an important question that deserves more investigation.

Along the Himalayan orogen, leucogranites are dominantly typical leucogranites (quartz + plagioclase + K-feldspar + muscovite), with subordinate biotite-bearing (also called two-mica granite), tourmaline-bearing, and garnet-bearing leucogranites. In the Malashan-Gyirong area of southern Tibet, plutons, dikes, and veins of leucogranitic compositions intruded into granitic gneiss, metapelite, marble, and unmetamorphosed Tethyan sediments. Gao and Zeng (2014) reported that the Malashan two-mica granites are derived from fluid-fluxed melting of muscovite, whereas the Paiku composite leucogranitic pluton was argued to be a product instead of fluid-absent melting of muscovite (Gao et al., 2013). Here, we report major and trace element concentrations and isotope ratios of Sr, Nd, and Hf in 74 leucogranite samples, together with published data from 87 leucogranite samples (Gao et al., 2013; Gao and Zeng, 2014; Wang et al., 2015), painting a detailed picture of the geochemical systematic variations in not only major elements and LILEs, but also HFSE and REE signatures of fluid-fluxed and fluid-absent melting of muscovite in metapelitic sources.

GEOLOGICAL SETTING

The Himalayan leucogranites are mainly distributed along two subparallel belts, the Tethyan Himalaya and the High Himalaya (Fig. DR1A in the GSA Data Repository[1]), separated by the Southern Tibetan detachment system (STDS). The study area, located in the central Himalayan orogenic belt, encompasses the Malashan Gneiss Dome within the Tethyan Himalaya, the STDS, and a segment of the High Himalayan belt (Fig. DR1B). The Malashan Dome consists of the Malashan and Cuobu two-mica granite, and the Paiku composite leucogranite in the core and pelitic and calcareous schist toward the margin. Within the STDS, there are leucogranites intruded into mylonitized granitic gneisses; most are strongly foliated. In the High Himalaya, undeformed leucogranites intruded into the High Himalayan Crystalline Sequence. The geochemical nature and formation mechanism of these leucogranites

in the STDS and High Himalaya have not been described before. In the study area, we sampled 180 leucogranites representing all the geologic units. In order to interpret bulk leucogranite chemistry as a probe of anatectic processes, it is necessary to eliminate, as much as possible, complexity due to effects such as peritectic or entrained K-feldspar, entrained plagioclase and biotite, and fractional crystallization. Hence, we developed filters based on careful evaluation of mineral assemblages, Eu and heavy (H) REE contents, and Rb/Sr and Nb/Ta ratios (Table DR1). As a result, we selected 74 out of 180 leucogranite samples for further discussion.

RESULTS

The leucogranite samples may be divided into two groups from both the Tethyan Himalaya and High Himalaya on the basis of numerous geochemical indicators. Group A contains leucogranites T0655, T0656, T0815-A, T0815-C, and previously published sample T0659 (Gao et al., 2013). Group B contains leucogranites T0649, T0651, T0804, T1021, T1022, T1023, ZC09, previously published sample TMLS (Gao and Zeng, 2014), and data from Wang et al. (2015). All the samples have high SiO_2 (69.7–77.1 wt%) and Al_2O_3 (12.9–16.2 wt%), but low CaO (<2.0 wt%), FeO* (<2.0 wt%), MgO, MnO, and TiO_2 (<0.31 wt%; Table DR2). Compared to group B, group A samples have relatively lower CaO (<1.0 wt%), FeO* (<1.0 wt%), and TiO_2 (<0.13 wt%; Fig. 1B; Figs. DR2A–DR2C). Na_2O/K_2O (in wt%) in most samples is less than 1.0 (Fig. 1B). In the albite (Ab)–anorthite (An)–orthoclase (Or) ternary diagram, all samples fall in the granite field, but group B samples are relatively higher in Ab than those in group A (Fig. 1A).

In primitive mantle–normalized spider diagrams (Figs. DR3A and DR3B), most rocks in group A share similar geochemical characteristics, with striking negative anomalies in Ba and Th alongside slightly negative anomalies in Sr and Ti. In contrast, most samples in group B are characterized by slightly negative anomalies in Ba, Sr, P, Nb, Ta, and Ti. Group A is characterized by relatively low Sr (<76 ppm), Ba (50–263 ppm), and Sr/Y (<6.6; Fig. DR2D), but high Rb (273–508 ppm) and Rb/Sr ratios greater

than 4.6 (up to 18.9; Fig. 1D). The Ba contents are negatively correlative with Rb/Sr ratios (Fig. 1D), which is considered to be a distinctive feature of fluid-absent melting of muscovite (Inger and Harris, 1993). Compared with group A, group B samples have higher Sr (105–300 ppm; Fig. 1C), Ba (305–1731 ppm), and Sr/Y (>3.5, up to 33.5; Fig. DR2D), but lower Rb (65–287 ppm) and Rb/Sr ratio (<2.2; Fig. 1D), and they are defined by nearly constant Rb/Sr ratios despite large variations in Ba concentrations (Fig. 1D), which are typical characteristics of fluid-fluxed melting of muscovite (Inger and Harris, 1993). Group A has higher Nb (6.7–18.4 ppm) and Ta (0.7–4.7 ppm) than group B (Nb <11.2 ppm, Ta <2.6 ppm; Fig. 2B); however, Nb/Ta ratios in group A are similar to those in group B, 3.1–10.3 and 2.3–13.6, respectively (Fig. DR2E). Zr, Hf, and Zr/Hf ratios in group A are lower than in group B (Fig. 2C). Group A has subchondritic Zr/Hf values (17.0–33.5), while group B covers a relatively wide range of Zr/Hf ratio (19.7–44.6), from subchondritic to slightly superchondritic (Fig. DR2F). Th and U compositions are also different. Group A has higher U (1.8–32.6 ppm), but lower Th (2.5–9.4 ppm; Fig. 2E) and lower Th/U ratio (<4.6) than group B. U and Th concentrations in group B range from 0.6 to 5.4 ppm and from 1.1 to 25.7 ppm, respectively, and Th/U ratios are up to 8.7 (Fig. DR2F).

The existence of entrained plagioclase and peritectic K-feldspar, as well as fractional crystallization of plagioclase and K-feldspar, could strongly affect the Eu anomalies. We only selected samples with Eu/Eu* ranging from 0.4 to 1.4, which could be original melts. All the leucogranites are enriched in light REEs (LREEs) and depleted in heavy REEs, with $(Gd/Yb)_N$ = 0.9–6.3 (Fig. 2A). The Eu anomalies display significant variations (Fig. 2A). Compared to group A, which is characterized
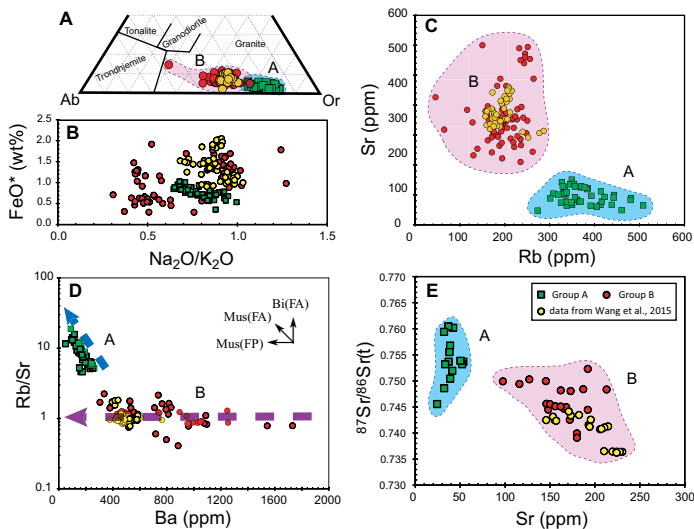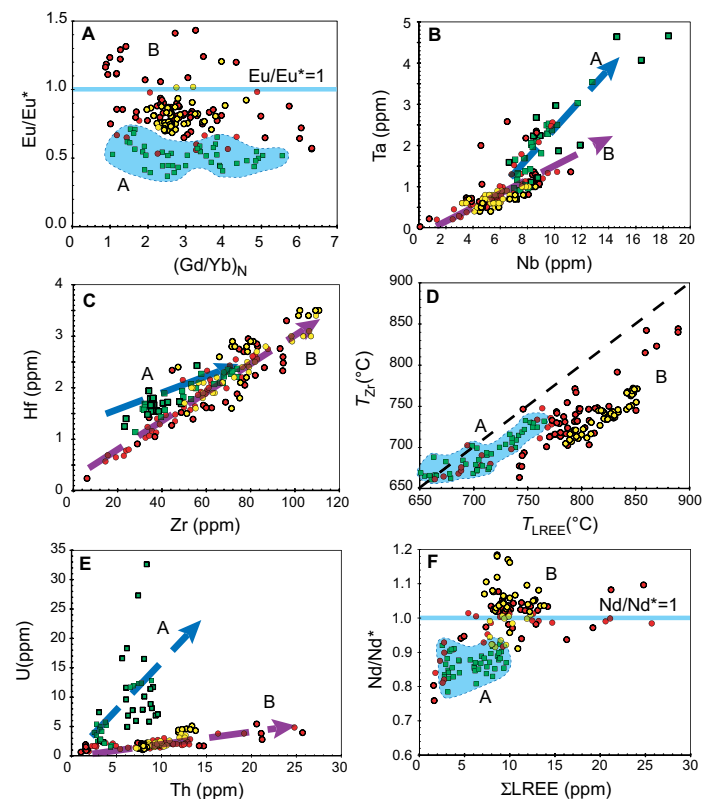

Figure 1. Major elements, trace elements, and isotopic characteristics of Himalayan leucogranite suite. A: Normative albite (Ab)–anorthite (An)–orthoclase (Or) contents. B: Na_2O/K_2O vs. total Fe as FeO*. C: Rb vs. Sr. D: Ba vs. Rb/Sr. E: $^{87}Sr/^{86}Sr(t)$ vs. Sr. Samples from the present study are grouped into two populations: group A and group B. Samples from Wang et al. (2015) invariably cluster with group B. In D, experimental trends for fluid-absent (FA) melting, dominated by biotite (Bi) and muscovite (Mus), and fluid-present (FP) melting, dominated by muscovite, are shown by the small black vectors (Inger and Harris, 1993).

Figure 2. Additional trace element concentrations, ratios, and trace element–based thermometers for Himalayan leucogranite suite. A: $(Gd/Yb)_N$ vs. Eu/Eu*. B: Nb vs. Ta. C: Zr vs. Hf. D: Saturation thermometry T_{LREE} (where LREE is light rare earth element) vs. T_{Zr}. E: Th vs. U. F: ΣLREE vs. Nd/Nd*. Symbols for group A, group B, and Wang et al. (2015) data are as in Figure 1. Compared to group A, group B has relatively low Nb, Ta, and U, but high Zr, Hf, Th, and LREE concentrations, together with high Zr/Hf, and positive Eu/Eu* and Nd/Nd* anomalies.

by Eu/Eu* ≤0.7, group B has relatively higher and more variable Eu anomalies (Eu/Eu* = 0.5–1.4). Similar to Eu anomalies, group B is defined by widely variable Nd anomalies [represented by Nd/Nd* = $Nd_N/[(Pr_N^2 \times Sm_N)^{1/3}]$, where N = chondrite-normalized], ranging from negative to positive, with Nd/Nd* mostly in the range 0.8–1.3. On the other hand, group A has limited negative Nd anomalies with Nd/Nd* = 0.8–0.9 (Fig. 2F).

The leucogranites display large variations in Sr and Nd isotope ratios, but all feature relatively radiogenic $^{87}Sr/^{86}Sr(t)$ (0.7364–0.7604) and unradiogenic $\varepsilon_{Nd}(t)$ (–12.3 to –15.3; Table DR3). Group A populates the high end of the $^{87}Sr/^{86}Sr$ range, with ratios ranging from 0.7456 to 0.7602, whereas group B is restricted to lower $^{87}Sr/^{86}Sr$ ratios (<0.7523). These isotopic differences, alongside the distinctive Sr contents of each group (Fig. 1E), are comparable to experimental results for fluid-absent and fluid-fluxed melting of a metapelitic source reported by Knesel and Davidson (2002). Hf isotope ratios in the two groups are different (Fig. DR4). On the magmatic zircon rims, group A is characterized by higher $\varepsilon_{Hf}(t)$ (–15.0 to –2.8) than group B (–24.9 to –8.0). Zircon cores from both groups show highly heterogeneous, substantially similar but more negative Hf isotope compositions, ranging from –34.9 to –7.6 and from –47.1 to –9.5 for group A and group B, respectively.

DISCUSSION

The FeO*, MgO, CaO, MnO, and TiO_2 contents almost overlap with those of melts produced by experiments at temperatures of 750–900 °C (Patiño Douce and Harris, 1998). This agreement suggests that most of these leucogranites are nearly pure liquid compositions. Although there were garnets in some highly fractionated samples, which we have excluded in this study, the garnets had high spessartine (at least 14%, up to 54%) and crystallized from later highly fractionated melts, different from peritectic garnet with spessartine lower than 10% (Patiño Douce and Harris, 1998). Therefore, we can rule out the possibility of biotite being a melting reactant.

The major elements, LILEs, and isotopic characteristics of the leucogranites clearly divide the samples into two groups. Group A displays all the characteristics expected from products of fluid-absent melting of muscovite, whereas group B displays all the characteristics associated with products of fluid-fluxed melting of muscovite (Fig. 1). Theoretical calculations and experimental results suggest that the differences in the melt concentrations of Ca, Rb, Sr, and Ba, as well as Rb/Sr and $^{87}Sr/^{86}Sr$ ratios, are controlled by the relative mass fractions of mica and feldspar consumed by the melting reaction. Fluid-fluxed melting consumes plagioclase in greater proportions than muscovite, and thus produces melts with higher Sr, Ba, Ca, and Sr/Y but lower Rb, Rb/Sr, and $^{87}Sr/^{86}Sr$ than melts derived from fluid-absent melting. Fluid-absent melting of muscovite typically forms K-feldspar as a peritectic phase, in contrast to fluid-fluxed melting, where peritectic K-feldspar is missing, and the original melt contained all the Eu elements of the reactants. Thus, fluid-absent melting generates melt with a negative Eu anomaly (Fig. 2A), whereas a slightly more positive Eu anomaly in the melt suggests fluid-fluxed melting. All these considerations suggest that the proportions of reactant phases (e.g., mica vs. feldspar) during progressive melting of a single source are determined by fluid availability or associated differences in melting temperatures, leading to predictable variations in key trace element contents and isotope ratios.

The concentrations of HFSEs (e.g., Nb, Ta, Ti, Zr, and Hf), other key elements (e.g., U, Th, and REEs), and their ratios (e.g., Zr/Hf, Nb/Ta) may also be used to divide the leucogranites into two groups (Fig. 2), which correlate with indicators of fluid-fluxed versus fluid-absent melting that we have attributed to the stoichiometry and LILE chemistry of the principal minerals involved in the melting reaction. This indicates that there is distinction in the dissolution of the accessory phases hosting these trace elements.

Nb and Ta are considered to be geochemical twins due to their similar charge and ionic radii. However, Nb and Ta are compatible in Ti-rich mineral phases and micas and can be fractionated in evolved peraluminous granites by the presence of micas (Stepanov and Hermann, 2013) or by interaction with late magmatic fluids (Ballouard et al., 2016). In the Himalayan suite, group A has higher Nb and Ta concentrations than group B. The diversity could be explained by a larger proportion of muscovite as the reactant during fluid-absent than fluid-fluxed melting. Hence, more Nb and Ta were liberated into the fluid-absent derived melts, and less mica was available in the residual assemblage to sequester Nb and Ta (Harris et al., 1995). A systematic study of rutile/melt partition coefficients by Klemme et al. (2005) found that, in all cases, $D_{Ta} > D_{Nb}$ for rutile. Group A has low TiO_2 but similar Nb/Ta ratios to group B (Fig. DR2E). This implies that the selected original leucogranites did not experience significant fractional crystallization of Ti-rich mineral phases and hydrothermal alteration. Therefore, the differences in the Nb and Ta concentrations in the two types of leucogranites are controlled by the relative proportion of muscovite contributing to the melt during different crustal melting events.

Like the Nb-Ta pair, Zr and Hf have equal charge and similar ionic radii, and it might be expected that the Zr/Hf ratio of a magma series should remain constant. However, Zr/Hf ratios can be quite variable. Such variations have been attributed to fractional crystallization (Claiborne et al., 2006) or differential dissolution (Tang et al., 2014) of zircon, or fluid metasomatism (Bau, 1996). In the current data set, Zr and Hf contents and Zr/Hf ratios in group B are higher than group A (Fig. DR2F), but $\varepsilon_{Hf}(t)$ in the zircon magmatic rims in group B are lower than in group A (Fig. DR4B). There is no correlation between SiO_2 contents and Zr/Hf ratios in the two groups of leucogranites, which could rule out the possibility that fractional crystallization of zircon was a major factor controlling the Zr/Hf ratio. Additionally, the previous discussions have negated the possibility that hydrothermal alteration occurred during the evolution process. Therefore, the distinctions in Zr/Hf ratios could be explained by the "zircon effect" (Tang et al., 2014). Zircon solubility in silicate melts is controlled by temperature, crystal size, and the melt and solid phase composition. During different types of crustal anatexis, differential dissolution of zircons in the source would lead to isotopically distinct batches of melts. The $\varepsilon_{Hf}(t)$ values of the inherited zircons are substantially negative (Fig. DR4A). Thus, melting of inherited zircon would increase the Zr and Hf contents and Zr/Hf ratios, but decrease the $\varepsilon_{Hf}(t)$ of the melts. Therefore, differential dissolution of zircons during different partial melting events resulted in higher Zr, Hf, Zr/Hf, but lower $\varepsilon_{Hf}(t)$, in group B than in group A.

In addition, the concentrations of Th, U, and REEs are also distinct in the two groups of leucogranites. In monazite, the partition coefficients for Th are 30% higher than those for the LREEs, but partition coefficients for U are 4 to 23 times lower than for the LREEs (Stepanov et al. 2012). The principal carrier phases for Sm and Nd are apatite and monazite (Zeng et al., 2005). Group B is characterized by higher Th than group A, despite lower U concentrations (Fig. 2E). Th concentrations have strong positive correlation with LREE contents (Fig. DR2G), which is consistent with control by accessory monazite. Group B is defined by slightly negative to positive Nd anomalies, but group A has negative Nd anomalies (Fig. 2F). Moreover, Nd/Nd* shows a broad positive correlation with ΣLREE (Fig. 2F) in the overall leucogranite suite, but no correlation with P_2O_5 contents (Fig. DR2H). An excess of Nd over neighboring LREEs characterizes monazite, so these results are consistent with Th and LREE concentrations (but not the P_2O_5 budget), being dominated by variable dissolution of entrained monazite, which is favored during fluid-fluxed melting (Villaros et al., 2009). Based on the Zr and LREE concentrations in the two groups of leucogranites, the temperatures inferred from zircon saturation thermometry (T_{Zr}; Watson and Harrison, 1983; Boehnke et al., 2013) and from monazite saturation thermometry (T_{LREE}; Montel, 1993) are both higher in group B than in group A (Fig. 2D). This is entirely contrary to expectations and experimental data (Patiño Douce and Harris, 1998). However,

the presence of entrained zircons and monazites in both groups of leuco-granites suggests that most T_{Zr} and T_{LREE} results in this suite are not true melt temperatures. We conclude that group B has relatively higher Th and LREE compositions than group A due to wet, low-temperature conditions favoring monazite dissolution, and the anomalous readings of the Zr and LREE thermometers in the two groups are the result of entrained zircons and monazites captured into melts during different crustal melting events.

CONCLUSIONS

There are pronounced differences in the concentrations of the major elements (K, Na, Ca), LILEs (Rb, Sr, Ba), HFSEs (Zr, Hf, Nb, Ta, U, Th), and REEs, as well as in the Sr and Hf isotope ratios in melts derived from fluid-fluxed melting versus fluid-absent melting of muscovite in metasedimentary sources. The coherent differences among leucogranites in many geochemical indicators can be attributed to the same root cause, dissolution behavior of major and accessory minerals during different crustal melting events. This result could be a general feature that helps us to understand the processes of low-temperature partial melting in the continental crust.

REFERENCES CITED

Ballouard, C., Poujol, M., Boulvais, P., Branquet, Y., Tartese, R., and Vigneresse, J., 2016, Nb-Ta fractionation in peraluminous granites: A marker of the magmatic-hydrothermal transition: Geology, v. 44, p. 231–234, doi:10.1130/G37475.1.

Bau, M., 1996, Controls on the fractionation of isovalent trace elements in magmatic and aqueous systems: Evidence from Y/Ho, Zr/Hf and lanthanide tetrad effect: Contributions to Mineralogy and Petrology, v. 123, p. 323–333, doi:10.1007/s004100050159.

Boehnke, P., Watson, E.B., Trail, D., Harrison, T.M., and Schmitt, A.K., 2013, Zircon saturation re-revisited: Chemical Geology, v. 351, p. 324–334, doi:10.1016/j.chemgeo.2013.05.028.

Claiborne, L.L., Miller, C.F., Walker, B.A., Wooden, J.L., Mazdab, F.K., and Bea, F., 2006, Tracking magmatic processes through Zr/Hf ratios in rocks and Hf and Ti zoning in zircons: An example from the Spirit Mountain batholith, Nevada: Mineralogical Magazine, v. 70, p. 517–543, doi:10.1180/0026461067050348.

Gao, L.E., and Zeng, L.S., 2014, Fluxed melting of metapelite and the formation of Miocene high-CaO two-mica granites in the Malashan gneiss dome, southern Tibet: Geochimica et Cosmochimica Acta, v. 130, p. 136–155, doi:10.1016/j.gca.2014.01.003.

Gao, L.E., Zeng, L.S., Hou, K.J., Guo, C.L., Tang, S.H., Xie, K.J., Hu, G.Y., and Wang, L., 2013, Episodic crustal anatexis and the formation of the Paiku composite leucogranitic pluton in the Malashan Gneiss Dome, southern Tibet: Chinese Science Bulletin, v. 58, p. 3546–3563, doi:10.1007/s11434-013-5792-4.

Harris, N., and Massey, J., 1994, Decompression and anatexis of Himalayan metapelites: Tectonics, v. 13, p. 1537–1546, doi:10.1029/94TC01611.

Harris, N., Ayres, M., and Massey, J., 1995, Geochemistry of granitic melts produced during the incongruent melting of muscovite: Implication for the extraction of Himalayan leucogranite magmas: Journal of Geophysical Research, v. 100, p. 15,767–15,777, doi:10.1029/94JB02623.

Inger, S., and Harris, N., 1993, Geochemical constraints on leucogranite magmatism in the Langtang Valley, Nepal Himalaya: Journal of Petrology, v. 34, p. 345–368, doi:10.1093/petrology/34.2.345.

King, J., Harris, N., Argles, T., Parrish, R., and Zhang, H.F., 2011, Contribution of crustal anatexis to the tectonic evolution of Indian crust beneath southern Tibet: Geological Society of America Bulletin, v. 123, p. 218–239, doi:10.1130/B30085.1.

Klemme, S., Prowatke, S., Hametner, K., and Gunther, D., 2005, Partitioning of trace elements between rutile and silicate melts: Implications for subduction zones: Geochimica et Cosmochimica Acta, v. 69, p. 2361–2371, doi:10.1016/j.gca.2004.11.015.

Knesel, K.M., and Davidson, J.P., 2002, Insights into collisional magmatism from isotopic fingerprints of melting reactions: Science, v. 296, p. 2206–2208, doi:10.1126/science.1070622.

Montel, J.M., 1993, A model for monazite/melt equilibrium and the application to the generation of granitic magmas: Chemical Geology, v. 110, p. 127–146, doi:10.1016/0009-2541(93)90250-M.

Patiño Douce, A.E., and Harris, N., 1998, Experimental constraints on Himalayan anatexis: Journal of Petrology, v. 39, p. 689–710, doi:10.1093/petroj/39.4.689.

Prince, C., Harris, N., and Vance, D., 2001, Fluid-enhanced melting during prograde metamorphism: Journal of the Geological Society of London, v. 158, p. 233–241, doi:10.1144/jgs.158.2.233.

Stepanov, A.S., and Hermann, J., 2013, Fractionation of Nb and Ta by biotite and phengite: Implications for the "missing Nb paradox": Geology, v. 41, p. 303–306, doi:10.1130/G33781.1.

Stepanov, A.S., Hermann, J., Rubatto, D., and Rapp, R.P., 2012, Experimental study of monazite/melt partitioning with implications for the REE, Th and U geochemistry of crustal rocks: Chemical Geology, v. 300–301, p. 200–220, doi:10.1016/j.chemgeo.2012.01.007.

Tang, M., Wang, X.L., Shu, X.J., Wang, D., Yang, T., and Gopon, P., 2014, Hafnium isotopic heterogeneity in zircons from granitic rocks: Geochemical evaluation and modeling of "zircon effect" in crustal anatexis: Earth and Planetary Science Letters, v. 389, p. 188–199, doi:10.1016/j.epsl.2013.12.036.

Villaros, A., Stevens, G., Moyen, J., and Buick, I.S., 2009, The trace element compositions of S-type granites: Evidence for disequilibrium melting and accessory phase entrainment in the source: Contributions to Mineralogy and Petrology, v. 158, p. 543–561, doi:10.1007/s00410-009-0396-3.

Wang, X.X., Zhang, J.J., Yan, S.Y., Liu, J., Wang, J.M., and Guo, L., 2015, Age and formation mechanism of the Qiamangba two-mica granite in northern Himalaya: Chinese Journal of Geology, v. 50, p. 708–727.

Watson, E.B., and Harrison, T.M., 1983, Zircon saturation revisited: Temperature and composition effects in a variety of crustal magma types: Earth and Planetary Science Letters, v. 64, p. 295–304, doi:10.1016/0012-821X(83)90211-X.

Weinberg, R.F., and Hasalova, P., 2015, Water-fluxed melting of the continental crust: A review: Lithos, v. 212–215, p. 158–188, doi:10.1016/j.lithos.2014.08.021.

Zeng, L.S., Saleeby, J.B., and Asimow, P., 2005, Nd isotope disequilibrium during crustal anatexis: A record from the Goat Ranch migmatite complex, southern Sierra Nevada batholith, California: Geology, v. 33, p. 53–56, doi:10.1130/G20831.1.

Zeng, L.S., Gao, L.E., Xie, K.J., and Liu, J., 2011, Mid-Eocene high Sr/Y granites in the Northern Himalayan gneiss domes: Melting thickened lower continental crust: Earth and Planetary Science Letters, v. 303, p. 251–266, doi:10.1016/j.epsl.2011.01.005.

Zhang, H.F., Harris, N., Parrish, R., Kelley, S., Zhang, L., and Rogers, N., 2004, Causes and consequences of protracted melting of the mid-crust exposed in the North Himalayan antiform: Earth and Planetary Science Letters, v. 228, p. 195–212, doi:10.1016/j.epsl.2004.09.031.